Infrared spectra of the low-dimensional quantum magnet $SrCu_2(BO_3)_2$: Measurements and *ab initio* calculations

C. C. Homes,[1,2,*] S. V. Dordevic,[1,3] A. Gozar,[1] G. Blumberg,[4,5] T. Rõõm,[5] D. Hüvonen,[5] U. Nagel,[5] A. D. LaForge,[6] D. N. Basov,[6] and H. Kageyama[7]

[1]*Department of Condensed Matter Physics and Materials Science, Brookhaven National Laboratory, Upton, New York 11973, USA*

[2]*Laboratoire Photons et Matière, UPR-5 CNRS, ESPCI, 10 Rue Vauquelin, 75231 Paris Cedex 5, France*

[3]*Department of Physics, The University of Akron, Akron, Ohio 44325, USA*

[4]*Department of Physics and Astronomy, Rutgers University, Piscataway, New Jersey 08854, USA*

[5]*National Institute of Chemical Physics and Biophysics, Akadeemia tee 23, 12618 Tallinn, Estonia*

[6]*Department of Physics, University of California-San Diego, San Diego, La Jolla, California 92093, USA*

[7]*Department of Chemistry, Graduate School of Science, Kyoto University, Kyoto 606-8502, Japan*

(Received 16 June 2008; revised manuscript received 28 November 2008; published 4 March 2009)

The reflectance of the insulating quasi-two-dimensional quantum magnet $SrCu_2(BO_3)_2$ has been examined over a wide temperature and frequency range for light polarized parallel (*a* axis) and perpendicular (*c* axis) to the copper- and boron-oxygen sheets. The spectra have been measured for temperatures below the structural phase transition $T_s=395$ K for both polarizations; above T_s a limited study of the in-plane properties was undertaken in the far-infrared region only. Several new modes appear in the reflectance just below T_s along the *a* and *c* axes, while others are visible only for $T \ll T_s$. Below T_s, the intensity of some of the new modes displays little or no temperature dependence, while the intensity of some vibrations increases dramatically with decreasing temperature. *Ab initio* calculations have been performed for the room-temperature phase using density-functional theory, and the frequencies and atomic characters of the infrared-active phonons at the zone center were obtained using the direct method. The agreement between the calculated and experimentally observed frequencies is quite good, and assignments of the modes are discussed. The vibrational features that are observed only at low temperature appear to be magnetic in origin.

DOI: 10.1103/PhysRevB.79.125101 PACS number(s): 63.20.−e, 71.15.Mb, 72.15.Jf, 74.25.Gz

I. INTRODUCTION

The low-dimensional quantum magnet $SrCu_2(BO_3)_2$ has received a considerable amount of attention recently for its unusual magnetic properties.[1–10] In this system the zero magnetic-field spin gap of $\Delta=3$ meV separates the singlet ground state from the excited triplet states. The crystal has a tetragonal symmetry in which the copper, boron, and oxygen atoms are organized in two-dimensional sheets. The $S=1/2$ spins lie on the copper sites in the layers to form interacting spin dimers that are orthogonally connected.[11] This exotic spin-exchange topology results in an almost perfect realization of the Shastry-Sutherland model.[12] It has been suggested that this material is close to a quantum critical point that separates the gapped short-range dimer phase from a gapless long-range antiferromagnetically ordered Néel state.[4–6] Some evidence has been found in the magnetic susceptibility for a closing of the gap under hydrostatic pressure.[3]

The magnetic properties of this material have been investigated in detail using several different experimental techniques, including magnetic susceptibility,[1–3] nuclear magnetic resonance,[1,2] thermal conductivity,[13] specific heat,[14] and ultrasonic attenuation;[15,16] all give results that are consistent with the thermal excitation of triplet states across the spin gap. Below about 20 K the population of excited magnetic states begins to diminish and well-defined direct transitions between the singlet ground state and the lowest excited triplet states are observed in electron-spin resonance[17] and inelastic neutron scattering.[18–20] There have also been a number of optical studies. Raman scattering,[21–24] infrared transmission, and magnetoabsorption studies[25,26] have all been able to observe several excitations across the spin gap; magneto-optical studies have revealed a significant field dependence for the transitions across the spin gap.[23,26] These studies all draw attention to the coupling between the spins and the lattice, and in particular the ability of optical methods to probe this behavior; however, a detailed infrared study of this material has not yet been performed. Strong spin-phonon interactions are expected to manifest themselves as either anomalous frequency shifts with the onset of magnetic order or the appearance of Fano-type asymmetric line shapes.[27–35]

In this work we have measured the reflectance of $SrCu_2(BO_3)_2$ for different polarizations over a wide temperature and frequency range below the structural phase transition $T_s=395$ K (Ref. 36); above T_s only the in-plane properties were examined. The measurements have been performed on the crystals from the same batch as those used in recent Raman scattering[23] and infrared[25,26] experiments, allowing for direct comparison of results. The infrared spectra reveal an insulating character along both crystallographic directions, allowing a large number of phonon modes to be identified in both the *ab*-plane and *c*-axis spectra. The evolution of the vibrational spectra in this material is rather unusual; some new modes develop just below T_s, while others are visible only below ~250 K, and one peculiar mode at 443 cm^{-1} (55 meV) appears only below ~20 K. In addition, some vibrational modes increase in intensity with decreasing temperature, contrary to the expectation that the oscillator strength should remain constant.

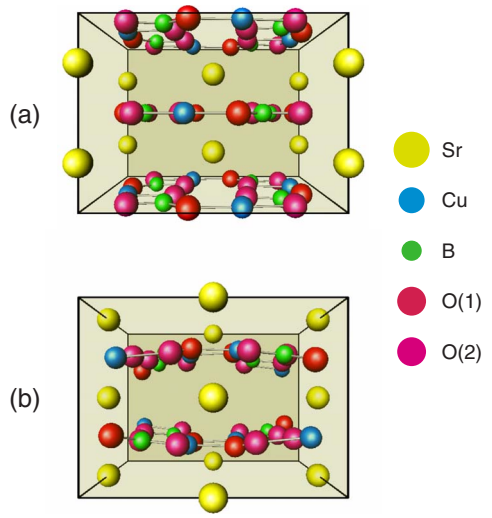

FIG. 1. (Color online) The unit cell of $SrCu_2(BO_3)_2$ in the (a) high-temperature $I4/mcm$ phase with coplanar copper and boron sheets, and (b) the low-temperature body-centered-tetragonal $I\bar{4}2m$ setting with $a=b=8.982$ Å and $c=6.643$ Å, showing the buckling of the copper- and boron-oxygen planes and loss of inversion symmetry (detailed structural parameters for the low-temperature phase may be found in Table II). The sheets describe the a-b planes, while the orthogonal direction is the c axis. The Sr atoms (yellow) lie between the Cu (blue) and B (green) sheets; the four-fold coordinated Cu atoms form a distorted square with the O(1) atoms (red), while the three-fold coordinated B also lies on the corner of a distorted square formed by the Cu and O(2) atoms (magenta).

To better understand the nature of the lattice vibrations in this complex material, *ab initio* calculations have been performed using density-functional theory, and the frequencies and atomic characters of the zone-center ($\mathbf{q}=0$) modes in the room-temperature structure have been determined using the direct method. The relative intensities of the infrared-active modes have also been calculated. The agreement between the predicted and observed frequencies is quite good. The modes that appear below T_s correspond to the predicted frequencies of the weak symmetry-allowed infrared modes. While there is no direct evidence for spin-phonon coupling in any of the infrared modes, there is evidence for a redistribution of charge within the unit cell at low temperature. In addition, the unusual temperature dependence of the 443 cm^{-1} mode suggests that it is probably a combination of a strong infrared mode and a magnetic excitation.

II. EXPERIMENT

$SrCu_2(BO_3)_2$ has a tetragonal symmetry in which layers of $(BO_3)^{3-}$ groups and Cu^{2+} ions are separated by closed-shell Sr^{2+} atoms. The a-b direction is along these planes (in plane) and c-axis direction is perpendicular to them (out of plane). At high temperature, this compound is in the $I4/mcm$ space group (D_{4h} point group) in which the copper and boron sheets are planar. The high-temperature phase is shown in Fig. 1(a), projected along the planes. Below $T_s=395$ K the system undergoes a displacive second-order phase transition to an $I\bar{4}2m$ space group (D_{2d} point group), in which the sheets buckle and the structure loses its inversion symmetry.[11,36] The room-temperature structure is shown in Fig. 1(b). This transition leads to an abrupt jump in the magnetic susceptibility at T_s (Ref. 4); however, the structure continues to evolve well below T_s and the fractional coordinates continue to show changes down to $T \lesssim 200$ K (Ref. 36).

Large single crystals of $SrCu_2(BO_3)_2$ have been grown by a traveling solvent floating zone method.[37] The crystals examined consisted of one with a cleaved a-b face and another which was oriented, cut, and polished to reveal an a-c face with an optically flat surface and a bright mirrorlike finish. Typical sample dimensions are $\sim 1 \times 2$ mm^2, with somewhat irregular perpendicular dimensions. The reflectance of the crystals of $SrCu_2(BO_3)_2$ has been measured between 5 and 295 K (below T_s) at a near-normal angle of incidence from $\sim$20 to 18 000 cm^{-1} using an *in situ* evaporation technique[38] with typical resolutions of 1 or 2 cm^{-1}. A more detailed temperature dependence up to 400 K ($T > T_s$) has been performed only in the far-infrared region for light polarized in the planes. For the crystal with an a-b face, the light was not polarized. In the case of the crystal with an a-c face, the reflectance has been measured using an s-polarized geometry for light polarized along the a and c axes. The s-polarized geometry has been employed because it has been demonstrated that it reduces the contamination from other crystallographic directions.[39]

III. RESULTS

The reflectance of $SrCu_2(BO_3)_2$ below 2000 cm^{-1} at 5 and 295 K for light polarized along the a and c axes is shown in Figs. 2(a) and 2(b), respectively. Due to the insulating character of this compound, the reflectance is dominated by the infrared-active vibrations, many of which sharpen considerably with decreasing temperature. In addition, some new features become visible in both polarizations only at low temperature.

The real and imaginary parts of the dielectric function have been calculated from a Kramers-Kronig analysis of the reflectance,[40] for which extrapolations are supplied for $\omega \rightarrow 0, \infty$. At low frequency, the reflectance is assumed to continue smoothly to $R \approx 0.2$; at high frequency, the reflectance is truncated at a cut-off frequency and above this point a free-electron approximation has been assumed ($R \propto \omega^{-4}$). The Kramers-Kronig analysis yields accurate information in the low-frequency region; however, the nature of the line shapes (profile and amplitude) observed in the imaginary part of the dielectric function above several hundred cm^{-1} are very sensitive to the choice of cut-off frequency and the nature of the high-frequency extrapolation. It seems likely that the frequency interval available in this experiment is insufficiently large for the Kramers-Kronig relation to yield accurate results over the entire region. For this reason, in order to quantitatively analyze the temperature dependence of phonon modes, we have chosen to fit the reflectance spectra to a model for the complex dielectric function ($\tilde{\epsilon}=\epsilon_1+i\epsilon_2$) consisting of Lorentz oscillators,

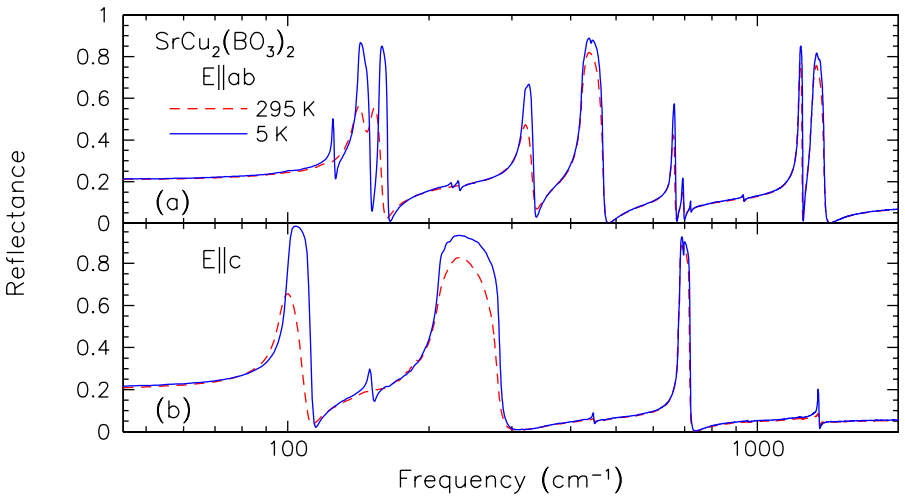

FIG. 2. (Color online) The temperature dependence of the reflectance of $SrCu_2(BO_3)_2$ versus the log of the frequency for (a) light polarized in the *a-b* planes and (b) light polarized along the *c* axis in the region of the infrared-active vibrations.

$$\tilde{\epsilon}(\omega) = \epsilon_\infty + \sum_j \frac{\omega_{p,j}^2}{\omega_j^2 - \omega^2 - i\gamma_j\omega}, \tag{1}$$

where ω_j, γ_j, and $\omega_{p,j}$ are the frequency, width, and effective plasma frequency of the jth vibration; ϵ_∞ is the high-frequency contribution to the dielectric function. The complex dielectric function is related to the complex refractive index $\tilde{n}=n+ik$,

$$n = \left[\frac{1}{2}(\sqrt{\epsilon_1^2+\epsilon_2^2}+\epsilon_1)\right]^{1/2} \tag{2}$$

and

$$k = \left[\frac{1}{2}(\sqrt{\epsilon_1^2+\epsilon_2^2}-\epsilon_1)\right]^{1/2}, \tag{3}$$

from which the reflectance at a normal angle of incidence can be calculated,

$$R = \frac{(n-1)^2+k^2}{(n+1)^2+k^2}. \tag{4}$$

The insulating nature of the spectra precludes any free-carrier contribution. The model reproduces the data very well, and the results of the fits to the reflectance at room temperature and 5 K for light polarized in the *a* and *c* axes are listed in Table I.

IV. DISCUSSION AND ANALYSIS

A. Vibrational features

The irreducible vibrational representations for both the high- and low-temperature phases of $SrCu_2(BO_3)_2$ have been previously examined[22,24] and will only be briefly discussed. In the high-temperature $I4/mcm$ phase, the presence of inversion symmetry allows the vibrations to be divided into even (g) and odd (u) species, yielding the vibrational representation

$$\Gamma_{\rm HT} = 5A_{1g} + 6A_{2g} + 5B_{1g} + 5B_{2g} + 6E_g + A_{1u} + 5A_{2u} + 4B_{1u} + B_{2u} + 11E_u,$$

including $A_{2u}+E_u$ acoustic modes. All of the even modes are Raman active. The odd A_{2u} and E_u modes are infrared active along the *c* axis and the planes, respectively. Below the structural phase transition at 395 K in the $I\bar{4}2m$ phase, the inversion symmetry is lost and it is no longer possible to label a species as even or odd. The irreducible vibrational representations at low temperature are

$$\Gamma_{\rm LT} = 9A_1 + 7A_2 + 6B_1 + 10B_2 + 17E,$$

including B_2+E acoustic modes. Effectively all of the 47 optical modes are Raman active.[24] The nine B_2 and 16E modes are infrared active with dipole moments along the *c* axis and the *a-b* planes, respectively.

It is clear from the irreducible vibrational representations that many more infrared-active modes should be observed in the *a-b* planes than along the *c* axis, and this is indeed what we observe in Fig. 2. Along the *c* axis at room temperature, we observe seven out of the nine possible B_2 modes. At low temperature these modes narrow considerably, and a sharp new mode is observed at 150 cm^{-1} (Table I). Within the *a-b* planes, the spectra are considerably more complicated. At room temperature, we observe only 10 out of the 16 possible E modes. At low temperature, in addition to the narrowing of most vibrational modes, new features are observed at 125, 223, 231, and 443 cm^{-1}, yielding a total of 14 modes. The detailed temperature dependence of the reflectance for light polarized along the *a* axis in the 120–170 cm^{-1} region is shown in Fig. 3(a); the reflectance has been modeled using the complex dielectric function in Eq. (1), and the fitted widths, frequencies, and effective plasma frequencies (the oscillator strength is proportional to $\omega_{p,j}^2$) of the modes as a function of temperature are shown in Fig. 4.

The behavior of the low-frequency vibrational modes may be seen more clearly in the imaginary part of the dielectric function (related to the optical absorption) shown in Fig. 3(b) that has been determined from a Kramers-Kronig analysis of the reflectance. Above T_s only one broad mode at about 142 cm^{-1} is observed. Below T_s the 157 cm^{-1} mode is immediately visible; however, the modes at 125, 223, and 231 cm^{-1} (shown in Figs. 2 and 3) only become visible below about 250 K (well below T_s). The imaginary part of the dielectric function for the mode at 443 cm^{-1}, shown in detail

TABLE I. The vibrational parameters for oscillator fits to the reflectance $SrCu_2(BO_3)_2$ for light polarized in the *a*-*b* planes and along the *c* axis at 295 and 5 K, where ω_j, γ_j, and $\omega_{p,j}$ are the frequency, width, and effective plasma frequency of the *j*th vibration. The value for the high-frequency contribution to the dielectric constant has been determined to be $\epsilon_{\infty,a}=3.4$ for the *a*-*b* planes and $\epsilon_{\infty,c}=2.7$ along the *c* axis. All units are in cm^{-1}, except for the dimensionless oscillator strength $S_j=\omega_{p,j}^2/\omega_j^2$; a value of zero indicates $S_j<0.01$.

$E\|a$							
295 K				5 K			
ω_j	γ_j	$\omega_{p,j}$	(S_j)	ω_j	γ_j	$\omega_{p,j}$	(S_j)
1307	16.4	763	(0.34)	1308	11.9	751	(0.33)
1226	4.4	601	(0.24)	1228	2.7	610	(0.25)
934	4.4	52	(0.01)	934	4.5	62	(0.01)
719	3.4	34	(0.00)	721	2.2	47	(0.00)
693	5.8	105	(0.02)	693	4.6	116	(0.03)
659	6.3	220	(0.11)	661	3.9	231	(0.12)
				443	4.0	35	(0.01)
425	6.5	386	(0.82)	424	4.1	394	(0.86)
318	12.2	254	(0.64)	319	5.4	257	(0.65)
				231	2.0	29	(0.02)
				223	2.5	23	(0.01)
150	5.2	94	(0.39)	157	0.7	76	(0.23)
142	4.7	140	(0.97)	141	1.8	150	(1.13)
				125	1.0	49	(0.15)
$E\|c$							
295 K				5 K			
1349	11.1	139	(0.01)	1347	7.7	203	(0.02)
956	5.2	19	(0.00)	955	4.3	29	(0.00)
694	5.7	30	(0.00)	696	2.2	30	(0.00)
682	2.4	360	(0.27)	683	1.9	350	(0.26)
449	5.7	30	(0.01)	448	3.1	40	(0.01)
211	10.1	318	(2.27)	211	4.2	331	(2.46)
				150	2.7	49	(0.11)
97	4.8	121	(1.55)	100	0.5	126	(1.58)

in Fig. 5, has a more unusual temperature dependence with an onset of absorption only below ~20 K, similar to another in-plane mode observed at 52 cm^{-1} in magnetoabsorption experiments.[25] In contrast, the modes above about 500 cm^{-1} in either polarization vary little with temperature (Table I).

The behavior of the three modes in the 120–170 cm^{-1} region may be considered as a template for other activated modes in this material, which along with the 443 cm^{-1} mode will be examined in more detail below. As Figs. 3(b) and 4(a) indicate, above T_s only one vibrational mode at about 141 cm^{-1} may be identified; just below T_s a new mode splits off of the main feature, narrowing rapidly and increasing in frequency with decreasing temperature until it may be clearly resolved at about 157 cm^{-1} for $T \ll T_s$. The original mode at 142 cm^{-1} narrows with decreasing temperature but otherwise displays little temperature dependence. It is interesting to note that in Fig. 4(c) the 142 cm^{-1} mode undergoes an abrupt decrease in oscillator strength below T_s. However, below T_s the sum of the oscillator strengths of the 141 and 157 cm^{-1} modes (dotted line) is roughly equal to that of the single mode above T_s, indicating that there is a conservation of oscillator strength between these modes across the structural phase transition. This suggests that above T_s both modes are optically active; however, they are degenerate in frequency.

Below about 250 K a weak mode is visible in Fig. 3(a) at ~121 cm^{-1}, increasing to 125 cm^{-1} at low temperature. The size and temperature dependences of the widths of the modes between 120 and 170 cm^{-1} are all comparable, as shown in Fig. 4(b), narrowing with decreasing temperature. However, unlike the two modes at slightly higher frequency which display effectively no temperature change in oscillator strength below T_s, the strength of the 125 cm^{-1} mode increases gradually below about 250 K, as shown in Fig. 4(c). A similar trend has been observed for the *c*-axis B_2 mode at 150 cm^{-1}. This behavior is unusual because while it is common for the frequency and width of a new mode that develops below a structural phase transition to change with de-

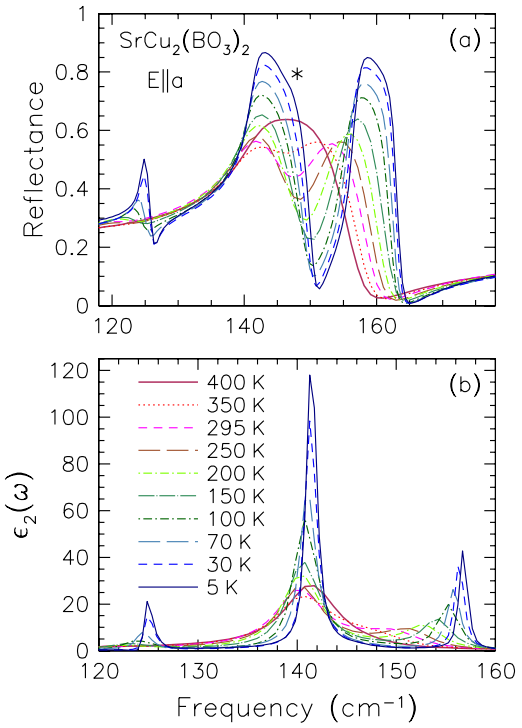

FIG. 3. (Color online) The detailed temperature dependence of (a) the reflectance of $SrCu_2(BO_3)_2$ above and below the structural phase transition at T_s=395 K for light polarized along the *a* axis in the region of the three low-frequency *E* lattice vibrations and (b) the imaginary part of the dielectric function. The asterisk in the upper panel denotes the appearance of a shoulder in the reflectance at low temperature. The experimental resolution is 2 cm^{-1}, except below 100 K, where it is 1 cm^{-1}. Note: the frequency intervals in the upper and lower panels are different.

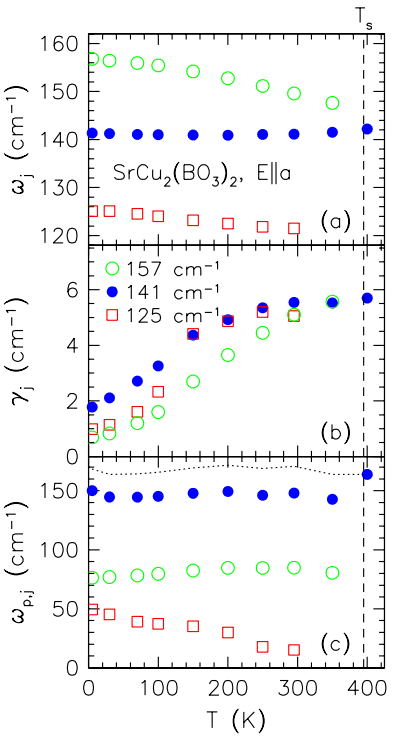

FIG. 4. (Color online) The temperature dependence of the fitted vibrational parameters of $SrCu_2(BO_3)_2$ for light polarized along the *a* axis for the (a) fundamental frequencies ω_j, (b) widths γ_j, and (c) effective plasma frequencies $\omega_{p,j}$ for the in-plane modes in the 120–170 cm^{-1} region. The solid circles track the mode visible in the high-temperature phase designated as the 141 cm^{-1}, while the open squares and circles represent vibrational modes at 125 and 157 cm^{-1}, respectively, that are observed below T_s (dashed line). The dotted line represents the sum of the oscillator strengths obtained through addition in quadrature of the effective plasma frequencies for the two modes at 141 and 157 cm^{-1}. The errors associated with the fitted results are comparable to the size of the symbols.

creasing temperature, the oscillator strength is expected to remain constant. We remark here that the rather gradual nature of the phase transition may make it difficult to initially observe weak new modes; however, while some changes might be explained by the evolution of the structure, below ~200 K no further changes are expected in this material as it has essentially achieved its final geometry.[36]

The activation of some modes at low temperature is even more exaggerated in the case of the 443 cm^{-1} mode, which is seen only as a weak antiresonance superimposed on a much stronger feature in the in-plane reflectance in Fig. 2(a) at 5 K. The temperature dependence of the imaginary part of the dielectric function for the 443 cm^{-1} mode is shown below 50 K in Fig. 5(a). The intensity of this mode has been estimated from the area under the curve (spectral weight) assuming a linear background; the relative intensity is shown in Fig. 5(b). This feature may only be identified below 20 K, which happens to coincide to the temperature at which magnetic transitions from the singlet to triplet states are first observed.

The behavior of these modes, and the development of the 443 cm^{-1} mode below ~20 K, indicates that in order to assign these features we must first understand the character of the vibrations. To obtain this information, we have undertaken a first-principles calculation of the lattice dynamics of the low-temperature phase, which we describe in Sec. IV B.

B. Calculation of phonon modes

The phonon frequencies were determined from first principles using the direct method,[41] in which the dynamical matrix is derived from the Hellmann-Feynman force constants arising when a single atom is displaced from its equilibrium position. The forces are calculated using density-functional theory with local-density approximation (LDA) exchange-correlation potential. The calculations for $SrCu_2(BO_3)_2$ were limited to the low-temperature $I\bar{4}2m$ space group with 44 atoms in the unit cell.

The initial step in this procedure is to determine the equilibrium volume and geometry for which the forces on each atom in the unit cell are minimized. The *ab initio* calculations on $SrCu_2(BO_3)_2$ were performed using the full-potential linearized augmented plane-wave (FP-LAPW) method[42] with local-orbital extensions[43] in the WIEN2K implementation.[44] In this treatment it is assumed that the material is paramagnetic and that the spins do not interact;

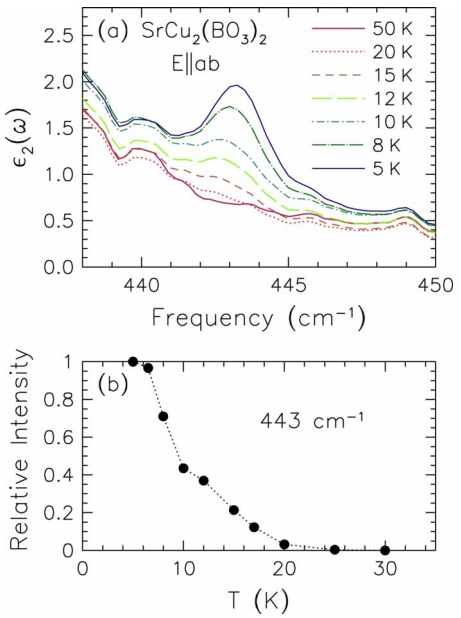

FIG. 5. (Color online) The detailed temperature dependence of (a) the imaginary part of the dielectric function of $SrCu_2(BO_3)_2$ for light polarized in the *a*-*b* planes in the region of the mode at 443 cm^{-1} below 50 K and (b) the relative intensity of the mode at 443 cm^{-1} below 35 K.

however, since the spins in the ground state are in fact correlated this approach may overlook forces generated by the coupling of spins. Within the scope of this calculation such effects are assumed to be weak, although this is not necessarily the case.[45,46] Studies with different Monkhorst-Pack *k*-point meshes indicated that a $2\times2\times2$ mesh was sufficient for good energy convergence. During the geometry optimization, the c/a ratio was fixed to the experimentally determined value.[36] Further geometric optimization was achieved by refining the atomic fractional coordinates within the unit cell until the total force on each of the atoms is typically less than 0.1 mRy/a.u. The results of the volume and geometry optimization are summarized in Table II. The geometry optimization yields values for the lattice constants that are in good agreement with the experimentally determined values.[36] The calculated total energy versus volume is illustrated in Fig. 6. A bulk modulus of ~170 GPa is extracted by fitting to the Murnaghan[47] equation of state.

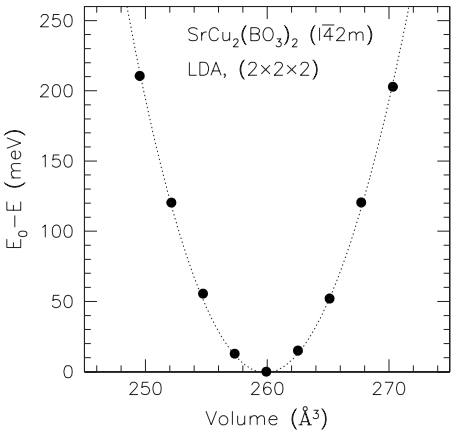

FIG. 6. Calculated total energy for the formula unit $SrCu_2(BO_3)_2$ in the low-temperature $I\bar{4}2m$ space group as a function of volume with constrained c/a ratio. The calculated equilibrium volume of 260 $Å^3$/f.u. is in good agreement with experimental value of 263 $Å^3$ (Ref. 36). The dotted line is a fit to the Murnaghan equation of state (Ref. 47).

The electronic band structure that is calculated from this optimized geometry reveals a nonzero density of states at the Fermi level, primarily from the Cu 3*d* orbitals (with a small contribution from O 2*p*), indicating metallic behavior. This is in contrast to the observed insulating character of this material, suggesting that a hybridized functional consisting of LDA plus an on-site repulsion U is required to accurately reproduce the band structure. Oscillator fits to the high-frequency reflectance for light polarized in the planes suggest that the charge-transfer gap is $\Delta_0 \simeq 0.7$ eV, indicating that this system should be viewed as a Mott insulator.[48] In a system such as this one where there are many valence electrons, there are many fully occupied bond states that contribute significantly to the binding energy between atoms, and therefore the forces; these are not directly related to the density of states at the Fermi level that determine the transport properties. Therefore, LDA alone has been deemed sufficient to calculate the forces.

TABLE II. Experimental and theoretical lattice constants and atomic fractional coordinates for the optimized structure of $SrCu_2(BO_3)_2$ for the low-temperature body-centered-tetragonal $I\bar{4}2m$ space group (44 atoms in the unit cell and 5 nonequivalent displacive particles). Note that in the optimized structure c/a has not been allowed to vary.

	Experiment[a]			Theory (LDA)		
a (Å)		8.982			8.882	
c (Å)		6.643			6.569	
Sr $(0\frac{1}{2}0)$						
Cu (xyz)	0.1146	0.1146	0.2884	0.1171	0.1171	0.2843
B (xyz)	0.2947	0.2947	0.2400	0.2977	0.2977	0.2403
O1 (xyz)	0.4003	0.4003	0.2000	0.4043	0.4043	0.2053
O2 (xyz)	0.3279	0.1453	0.2568	0.3309	0.1470	0.2569

[a]Reference 36.

To determine the phonons at the zone center, a $1\times1\times1$ supercell is sufficient. To obtain a complete set of Hellmann-Feynman forces, a total of 12 independent displacements are required; we have considered symmetric displacements which doubles this number, resulting in 24 separate structure files. In this case, displacement amplitudes of 0.04 Å were used. Typical values for the displacements range from 0.02 to 0.06 Å; however, the displacements should be small enough to ensure that the response is still linear. The introduction of displacements also has the effect of lowering the symmetry of the system. For these calculations a $2\times2\times2$ k-point mesh was again chosen. After each structure has converged using the criteria that the total forces on each atom are less than 0.02 mRy/a.u., the residual forces are collected for each set of symmetric displacements and a list of the Hellmann-Feynman forces are generated. Using the program PHONON,[49] the cumulative force constants deconvoluted from the Hellmann-Feynman forces are introduced into the dynamical matrix, which is then diagonalized in order to obtain the phonon frequencies.

The relative intensities have been estimated by calculating the net dipole moment of the atomic displacements

$$\mu_i = \sum_j Z_j^* w_{ij}, \tag{5}$$

where Z_j^* is the Born effective charge of the jth atom in the unit cell and w_{ij} is its displacement in the ith direction. The square of each sum is considered to estimate the relative intensity for light polarized in the direction of that axis. In this instance, Z_j^* is simply assumed to be the full ionic charge for each atom.

The calculated E and B_2 phonon frequencies for $\mathbf{q}=0$ are compared in Table III with the corresponding infrared-active vibrations observed at 5 K; the calculated relative intensities are listed and compared with the experimentally measured quantities (recall that the oscillator strength is proportional to $\omega_{p,j}^2$). The overall agreement between experiment ($T\ll T_s$) and theory is excellent, typically within a few percent, and there is good agreement between the observed strength of the vibrations and the calculated relative intensities. The atomic intensity for each vibrational mode is also listed (this quantity is the sum of the square of the vibrational amplitude of each atom over the allowed degrees of freedom). The atomic intensity characterizes the nature of the vibration. In compiling the experimentally observed frequencies in Table III, there are two E modes calculated to be at 76 and 112, as well as a B_2 mode at 313 cm^{-1}, that are not observed in the infrared reflectance spectra; this is not too surprising as the calculated relative intensities of these modes are predicted to be very weak. However, there are promising candidates in the Raman spectra[22,23] for these modes (indicated by parenthesis in Table III). While most of the vibrational assignments have been relatively straightforward, the modes at 693 and 721 cm^{-1} present a problem. The vibrations have been assigned to the modes calculated to be at 669 and 670 cm^{-1}; these modes are nearly degenerate in frequency and have a similar vibrational character. In addition, both modes are expected to be relatively strong. However, the experimentally observed modes are relatively weak, and the strength of the 721 cm^{-1} mode in particular appears to be somewhat sample dependent.

The relative atomic displacements for the 16 infrared-active E modes are shown in Fig. 7 for the upper copper- and boron-oxygen sheets in order to provide a visual representation of the atomic intensities listed in Table III and to illustrate the character of the modes more clearly. A dividing line in the character of the E (B_2) modes occurs at about 500 cm^{-1}. The modes observed at 661, 693, 721, 934, 1228, and 1308 cm^{-1} are predicted to consist almost entirely of boron and oxygen displacements, and the modes observed at 424 and 443 cm^{-1} are predicted to consist mainly of copper and oxygen displacements. The modes observed at 231 and 319 cm^{-1} retain a boron-oxygen character. The remaining low-frequency E modes vary greatly in nature. The modes observed at 157 and 223 cm^{-1} are predicted to be primarily copper-oxygen vibrations, while the mode observed at 141 cm^{-1} is similar but has a significant strontium character. The mode observed at 125 cm^{-1} is predicted to be mainly a strontium-oxygen vibration. The remaining two low-frequency E modes are calculated to have zero intensity and are observed using Raman spectroscopy at 80 and 112 cm^{-1}; these modes are predicted to involve displacements of mainly the strontium and copper atoms. It is important to note that the atomic displacements shown in Fig. 7 are not necessarily restricted to the copper- and boron-oxygen sheets; out-of-plane displacements are also observed. However, there are two sheets in the unit cell and the resultant dipole moment is found to lie solely within the a-b planes.

From Fig. 3 and Table I we note the general absence of any strong phonon frequency shifts through the phase transition or at low temperature (typically only a few cm^{-1}) or asymmetric phonon line shapes; this suggests that insofar as the infrared-active modes are concerned, the spin-phonon coupling in this compound is quite weak.

C. Low-frequency modes

It is interesting to once again examine the nature of the three modes at 125, 141, and 157 cm^{-1} at low temperature, where the character of the 125 cm^{-1} mode is quite different than the other two. The strong fundamental mode at 141 cm^{-1} consists of Sr/Cu-O(1) motions, while the 157 cm^{-1} mode consists mainly of Cu-O(2) displacements; however, a common feature of the 141 and 157 cm^{-1} modes is the torsional motion of different aspects of the copper-oxygen plaquette. The 125 cm^{-1} vibration is mainly a Sr–O(1)/O(2) mode that involves a rocking motion of the boron- and copper-oxygen plaquettes (in which the boron and copper are essentially stationary). The low-frequency mode at 125 cm^{-1} is distinctly different from the other two in that it does not involve significant copper-oxygen interactions. Perhaps the most peculiar aspect of the 125 cm^{-1} mode is the increase in oscillator strength with decreasing temperature. The intensity of an oscillator should be independent of temperature, as we observe for the 141 and 157 cm^{-1} modes in Fig. 4(c); variations in the intensity are usually associated with changes in the coordination or structure, or in the formal charges on the ions. While the 125 cm^{-1} mode is indeed

TABLE III. The experimentally observed ($T \sim 5$ K) and calculated phonon frequencies at the zone center of the infrared (and Raman) active E and B_2 modes for $SrCu_2(BO_3)_2$ in the tetragonal $I\bar{4}2m$ setting; the estimated numerical uncertainty in the calculation is roughly 5%. The E modes are active in the a-b plane, while the B_2 modes are active only along the c axis. (Those modes that are seen only in the Raman results are shown in parenthesis for the E modes at 80 and 112 cm^{-1} and the B_2 mode at 317 cm^{-1}.) The relative intensities of the modes have been calculated from the modulus of the induced dipole moments μ_i^2. The character of the mode is illustrated by the atomic intensities shown to the first two significant figures.

Mode	ω_{obs} [a] (cm^{-1})	ω_{calc} (cm^{-1})	$\lvert\mu^2_{i,calc}\rvert$ (rel.)	Atomic intensity				
				Sr	Cu	B	O(1)	O(2)
E	1308 s	1355	0.83	0.00	0.00	0.74	0.18	0.08
E	1228 s	1268	1.00	0.00	0.00	0.72	0.01	0.27
E	934 vw	932	0.00	0.00	0.00	0.00	0.35	0.65
E	721 vw	670	0.26	0.00	0.05	0.43	0.30	0.22
E	693 w	669	0.10	0.00	0.06	0.36	0.36	0.22
E	661 m	609	0.03	0.00	0.02	0.10	0.26	0.62
E	443 vw	442	0.00	0.00	0.23	0.04	0.10	0.63
E	424 s	392	0.21	0.00	0.28	0.06	0.17	0.49
E	319 m	299	0.01	0.03	0.02	0.23	0.12	0.60
E	231 vw	222	0.00	0.03	0.11	0.11	0.08	0.67
E	223 vw	204	0.01	0.01	0.60	0.03	0.17	0.19
E	157 vw	172	0.01	0.02	0.18	0.01	0.18	0.61
E	141 w	140	0.03	0.57	0.16	0.03	0.20	0.04
E	125 vw	129	0.01	0.21	0.06	0.04	0.38	0.31
E	(112)	112	0.00	0.37	0.53	0.00	0.02	0.08
E	(80)	76	0.00	0.51	0.32	0.04	0.02	0.11
B_2	1347 m	1361	0.02	0.00	0.00	0.72	0.21	0.07
B_2	955 vw	956	0.00	0.00	0.01	0.01	0.40	0.58
B_2	695 vw	641	0.00	0.00	0.04	0.14	0.16	0.66
B_2	682 s	642	1.00	0.00	0.00	0.79	0.06	0.15
B_2	447 vw	423	0.00	0.00	0.30	0.11	0.22	0.37
B_2	(317)	313	0.00	0.00	0.62	0.03	0.06	0.29
B_2	211 s	212	0.13	0.09	0.28	0.14	0.10	0.39
B_2	150 vw	165	0.00	0.16	0.12	0.00	0.50	0.22
B_2	101 w	99	0.00	0.48	0.26	0.00	0.23	0.03

[a]The qualitative descriptions of the strengths of the modes have been sorted in the following manner: very weak (vw), $\omega_{p,j} < 100$ cm^{-1}, weak (w), $\omega_{p,j} < 200$ cm^{-1}, and medium (m), $\omega_{p,j} < 300$ cm^{-1}; all other modes are labeled as strong (s).

associated with a structural phase transition, studies indicate that both the unit-cell dimensions and the fractional coordinates change very little below 200 K (Ref. 36), precisely the point where this mode begins to gather strength. It is possible that a redistribution of charge within the unit cell may be responsible for the increase in oscillator strength of this mode; however, one would also expect to see commensurate changes in the oscillator strengths of other modes with decreasing temperature. Such a condition is expressed through the relation[50]

$$\sum_j \omega_{p,j}^2 = \frac{4\pi\epsilon_\infty}{V_c} \sum_k \frac{(Z_k^* e)^2}{M_k}, \tag{6}$$

where $\Sigma_k Z_k^* = 0$, V_c is the unit-cell volume, and j and k index the lattice modes over all polarizations and the atoms with mass M_k, respectively. It is clear from an inspection of Table I that there is slightly more oscillator strength at $T \ll T_s$ than for $T \simeq T_s$. While the presence of several light ions prevents any estimate of the effective charge for a specific ion, the increase in oscillator strength supports the view that the material may become increasingly ionic at low temperature. Whatever mechanism is responsible for the increase in oscillator strength of the E mode at 125 cm^{-1}, it is likely that this is also responsible for the similar behavior of the E modes at 223 and 231 cm^{-1}, as well as the B_2 mode at 150 cm^{-1} which display a similar temperature dependence (see Table I).

We note in passing that in Fig. 3(a) the doubly-degenerate E mode at 141 cm^{-1} appears to develop a weak shoulder at low temperature (asterisk). This may suggest a further weak structural distortion that results in an additional lowering of

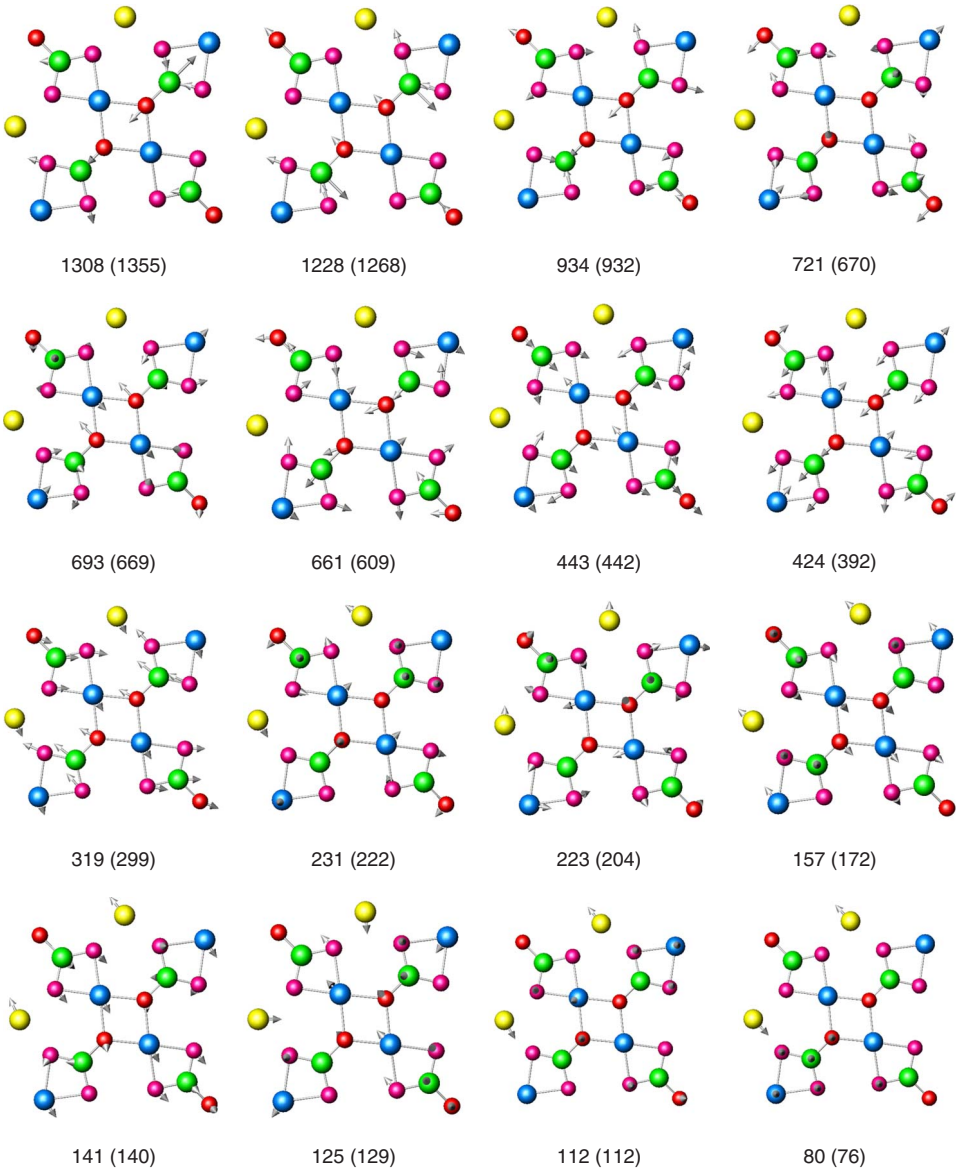

FIG. 7. (Color online) The calculated relative atomic displacements in the *a*-*b* planes for the 16 infrared-active *E* modes in $SrCu_2(BO_3)_2$; only the upper copper-boron sheet in the unit cell is shown. The observed frequency is shown below the displacements, with the calculated frequency indicated in parenthesis. The color scheme used to depict the atoms is taken from Fig. 1.

the symmetry and the removal of the degeneracy of this mode. However, at this time we are not aware of any high-resolution structural studies at low temperature that would support this claim.[51]

D. 443 cm^{-1} mode

The imaginary part of the dielectric function is shown in the vicinity of the mode at 443 cm^{-1} in Fig. 5(a) and the relative intensity in Fig. 5(b). Interestingly, there is no indication of a feature at this frequency above ~20 K; below this temperature this feature narrows and hardens only slightly. There are several possible explanations as to the origin of this feature; one is that it is simply the weak *E* mode calculated to be at 442 cm^{-1}. It is also possible that this feature is a combination of two other vibrations, such as the *E* mode at 319 cm^{-1} and a B_1 mode at 124 cm^{-1}, which sum to 443 cm^{-1}; note that in the D_{2d} point group $E \times (A_1, A_2, B_1) = E$, so this combination is an allowed infrared-active mode, although it is expected to be very weak. A third possibility is that this feature originates from the splitting of the strong *E* mode at 424 cm^{-1} due to a symmetry-breaking process; however, the lack of similar features in other strong modes makes this unlikely. These scenarios, while all are plausible to varying degrees, do not explain the unusual temperature dependence of this mode. The fact that the temperature dependence of the intensity of this feature is almost identical to those of the magnetic excitations, as well as the more general dc susceptibility,[20] suggests a possible magnetic origin for this feature. Since the exchange couplings $J \simeq 70$ cm^{-1} we may rule out a purely magnetic excitation. It is possible that this mode is a combination of the strong

424 cm^{-1} mode and a magnetic excitation, with the closest candidate being the singlet at $\simeq 21.5$ cm^{-1} observed in infrared magnetoabsorption[26] and high-field electron-spin resonance.[17] While the temperature dependence of this mode points to a magnetic origin, to properly determine whether this feature is a phonon or a combination of a phonon and a magnetic excitation, the magnetic-field dependence of the feature at 443 cm^{-1} should be investigated. Finally, we noted earlier in text that the temperature dependence of the 443 cm^{-1} mode was very similar to another in-plane mode observed at 52 cm^{-1}; however, there is compelling evidence that the 52 cm^{-1} feature is a pure magnetic mode.[25]

V. CONCLUSIONS

The reflectance of insulating $SrCu_2(BO_3)_2$ is dominated by the symmetry-allowed infrared lattice vibrations above and below the structural phase transition. In agreement with group theory, a number of new modes are observed below T_s. *Ab initio* calculations were performed using density-functional theory with LDA and the direct method to determine the frequencies, atomic character, and relative intensities of the infrared-active E and B_2 modes for the room-temperature phase ($T < T_s$) of this compound. The agreement between the calculated and experimentally observed frequencies (Table III) is excellent, and all the predicted modes have been identified.

The intensity of most of the infrared-active modes displays little temperature dependence (Table I). However, several modes, in particular an E mode at 125 cm^{-1} and a B_2 mode at 150 cm^{-1}, become visible only for $T \ll T_s$ and display a steadily increasing oscillator strength with decreasing temperature. This unexpected result suggests that a redistribution of charge within the unit cell occurs at low temperature. The absence of any large frequency shifts or asymmetric phonon line shapes suggests that, at least as far as the infrared-active vibrations are concerned, the spin-phonon coupling in this compound is very weak.

A weak mode at 443 cm^{-1} is observed only at low temperature and displays a similar temperature dependence to the magnetic excitations. This is similar to a feature at 52 cm^{-1}, previously observed in the infrared magnetoabsorption that has been identified as an electric-dipole transition in the dimer spin system. It is likely that the 443 cm^{-1} feature is a combination of a strong E mode at 424 cm^{-1} and a magnetic excitation. However, additional study of the magnetic-field dependence of this mode is required to determine if this is simply a phonon or a combination of a phonon and a magnetic excitation.

TABLE IV. The experimentally observed ($T \sim 5$ K) and calculated phonon frequencies at the zone center of the A_1, B_1, and A_2 Raman-active modes for $SrCu_2(BO_3)_2$ in the tetragonal $I\bar{4}2m$ setting; the estimated numerical uncertainty in the calculation is roughly 5%. The character of the mode is illustrated by the atomic intensities shown to the first two significant figures.

Mode	ω_{obs} (cm^{-1})	ω_{calc} (cm^{-1})	Atomic intensity				
			Sr	Cu	B	O(1)	O(2)
A_1	1360	1379	0.00	0.00	0.71	0.19	0.10
A_1	950	881	0.00	0.01	0.00	0.38	0.61
A_1		649	0.00	0.00	0.75	0.06	0.19
A_1		640	0.00	0.00	0.20	0.26	0.54
A_1	473	489	0.00	0.40	0.05	0.08	0.47
A_1	285	268	0.00	0.30	0.00	0.54	0.16
A_1	198	209	0.00	0.52	0.09	0.13	0.26
A_1	122	93	0.00	0.20	0.16	0.29	0.35
A_1	60	~ 0	0.00	0.57	0.04	0.07	0.32
B_1		1237	0.00	0.00	0.72	0.00	0.28
B_1	706	651	0.00	0.02	0.03	0.58	0.37
B_1	386	390	0.00	0.08	0.01	0.22	0.69
B_1	323	312	0.00	0.31	0.16	0.14	0.39
B_1	283	270	0.00	0.01	0.00	0.00	0.99
B_1	125	113	0.00	0.58	0.08	0.06	0.28
A_2		1267	0.00	0.00	0.71	0.01	0.28
A_2		593	0.00	0.00	0.03	0.73	0.24
A_2		457	0.00	0.17	0.00	0.09	0.74
A_2		300	0.07	0.01	0.23	0.12	0.57
A_2		227	0.01	0.00	0.01	0.00	0.98
A_2		196	0.91	0.01	0.02	0.01	0.05
A_2	156	156	0.01	0.81	0.00	0.05	0.13

ACKNOWLEDGMENTS

The authors would like to thank A. Akrap, B. D. Gaulin, J. Hancock, W. Ku, and T. Timusk for useful discussions. This work was supported by Grant-in-Aid for Scientific Research on Priority Areas from MEXT of Japan (Contract No. 19052004). Work at UCSD is supported by NSF Grant No. DMR 0705171; work at BNL is supported by the Office of Science, U.S. Department of Energy (DOE) under Contract No. DE-AC02-98CH10886.

APPENDIX: RAMAN MODES

The Raman-active A_1, B_1, and A_2 modes have also been calculated. The experimental values from the literature[22,23,36] are compared with the calculated frequencies in Table IV. The lack of high-frequency data results in a list of assigned frequencies that is not as comprehensive as in Table III. In general, the agreement between the calculated and observed frequencies appears to be quite good. In particular, the mode with A_1 symmetry observed at very low frequency just below T_s that hardens to about 60 cm^{-1} at low temperature[22,36] is likely the lowest-frequency A_1 mode. Similarly, the Raman mode at 124 cm^{-1} that had previously been assigned as an overtone[22] of this vibration now appears to be the next highest A_1 mode, although it must be said that the agreement with the calculated frequencies is less than ideal (better agreement would likely be achieved through the use of larger supercells in the calculations).

The assignment of the A_2 mode at 156 cm^{-1} is unusual as this mode is silent if phonon coupling alone is considered. However, if other processes are taken into account (i.e., spin-orbit interaction, etc.) then the resonant Raman-scattering process coupling to the antisymmetric A_2 modes is generally not forbidden. It is also possible that the mode at 156 cm^{-1} is not an A_2 mode at all but a combination of the fully symmetric A_1 mode at 122 cm^{-1} and an A_2 species triplet excitation at roughly 36 cm^{-1} (in the D_{2d} point group $A_1 \times A_2 = A_2$). However, this assignment remains rather speculative.

While there is little evidence for spin-phonon coupling in the infrared-active modes [see for instance Fig. 3(b), where the vibrations show a continuous hardening below 30 K], the A_1 mode observed at ~60 cm^{-1} does show a slight softening below about 15 K (Ref. 22). Indeed, our own unpublished Raman results[52] for this compound not only verify the softening in the A_1 mode at ~60 cm^{-1} but also identify a similar softening in another A_1 mode at 198 cm^{-1}. However, an A_1 mode at 122 cm^{-1} shows little change in frequency at low temperature. The difference in behavior of these modes may arise from the fact that the A_1 mode at 122 cm^{-1} is predicted to have a mixed copper- and boron-oxygen characters, while the A_1 modes at ~60 and 198 cm^{-1} have a primarily copper-oxygen character, suggesting that the weak softening of these vibrations at low temperature may be due to spin-phonon coupling.

*homes@bnl.gov

[1] H. Kageyama, K. Yoshimura, R. Stern, N. V. Mushnikov, K. Onizuka, M. Kato, K. Kosuge, C. P. Slichter, T. Goto, and Y. Ueda, Phys. Rev. Lett. **82**, 3168 (1999).

[2] H. Kageyama, K. Yoshimura, R. Stern, N. V. Mushnikov, K. Onizuka, M. Kato, K. Kosuge, C. P. Slichter, T. Goto, and Y. Ueda, J. Phys. Soc. Jpn. **68**, 1821 (1999).

[3] H. Kageyama, N. V. Mushnikov, M. Yamada, T. Goto, and Y. Ueda, Physica B **329-333**, 1020 (2003).

[4] S. Miyahara and K. Ueda, Phys. Rev. Lett. **82**, 3701 (1999).

[5] Zheng Weihong, C. J. Hamer, and J. Oitmaa, Phys. Rev. B **60**, 6608 (1999).

[6] E. Müller-Hartmann, R. R. P. Singh, C. Knetter, and G. S. Uhrig, Phys. Rev. Lett. **84**, 1808 (2000).

[7] A. Koga and N. Kawakami, Phys. Rev. Lett. **84**, 4461 (2000).

[8] K. Kodama, M. Takigawa, M. Horvatić, C. Berthier, H. Kageyama, Y. Ueda, S. Miyahara, F. Becca, and F. Mila, Science **298**, 395 (2002).

[9] S. Miyahara and K. Ueda, J. Phys.: Condens. Matter **15**, R327 (2003).

[10] M. Takigawa, S. Matsubara, M. Horvatic, C. Berthier, H. Kageyama, and Y. Ueda, Phys. Rev. Lett. **101**, 037202 (2008).

[11] R. W. Smith and D. A. Kesler, J. Solid State Chem. **93**, 430 (1991).

[12] B. Sriram Shastry and B. Sutherland, Physica B & C **108**, 1069 (1981).

[13] M. Hofmann, T. Lorenz, G. S. Uhrig, H. Kierspel, O. Zabara, A. Freimuth, H. Kageyama, and Y. Ueda, Phys. Rev. Lett. **87**, 047202 (2001).

[14] G. A. Jorge, R. Stern, M. Jaime, N. Harrison, J Bonca, S. E. Shawish, C. D. Batista, H. A. Dabkowska, and B. D. Gaulin, Phys. Rev. B **71**, 092403 (2005).

[15] S. Zherlitsyn, S. Schmidt, B. Wolf, H. Schwenk, B. Lüthi, H. Kageyama, K. Onizuka, Y. Ueda, and K. Ueda, Phys. Rev. B **62**, R6097 (2000).

[16] B. Wolf, S. Zherlitsyn, S. Schmidt, B. Lüthi, H. Kageyama, and Y. Ueda, Phys. Rev. Lett. **86**, 4847 (2001).

[17] H. Nojiri, H. Kageyama, Y. Ueda, and M. Motokawa, J. Phys. Soc. Jpn. **72**, 3243 (2003).

[18] H. Kageyama, M. Nishi, N. Aso, K. Onizuka, T. Yosihama, K. Nukui, K. Kodama, K. Kakurai, and Y. Ueda, Phys. Rev. Lett. **84**, 5876 (2000).

[19] O. Cépas, K. Kakurai, L. P. Regnault, T. Ziman, J. P. Boucher, N. Aso, M. Nishi, H. Kageyama, and Y. Ueda, Phys. Rev. Lett. **87**, 167205 (2001).

[20] B. D. Gaulin, S. H. Lee, S. Haravifard, J. P. Castellan, A. J. Berlinsky, H. A. Dabkowska, Y. Qiu, and J. R. D. Copley, Phys. Rev. Lett. **93**, 267202 (2004).

[21] P. Lemmens, M. Grove, M. Fischer, G. Güntherodt, V. N. Kotov, H. Kageyama, K. Onizuka, and Y. Ueda, Phys. Rev. Lett. **85**, 2605 (2000).

[22] K.-Y. Choi, Y. G. Pashkevich, K. V. Lamonova, H. Kageyama, Y. Ueda, and P. Lemmens, Phys. Rev. B **68**, 104418 (2003).

[23] A. Gozar, B. S. Dennis, H. Kageyama, and G. Blumberg, Phys. Rev. B **72**, 064405 (2005).

[24] A. Gozar and G. Blumberg, in *Frontiers in Magnetic Materials*,

edited by A. V. Narlikar (Spinger-Verlag, Berlin, 2005), pp. 735-754; this work was originally made available online at arXiv:cond-mat/0509630.
[25] T. Rõõm, U. Nagel, E. Lippmaa, H. Kageyama, K. Onizuka, and Y. Ueda, Phys. Rev. B **61**, 14342 (2000).
[26] T. Rõõm, D. Hüvonen, U. Nagel, J. Hwang, T. Timusk, and H. Kageyama, Phys. Rev. B **70**, 144417 (2004).
[27] J. W. Bray, L. V. Iterrante, I. S. Jacobs, and J. C. Bonner, in *Extended Linear Chain Compounds*, edited by J. S. Miller (Plenum, New York, 1983), pp. 353-415.
[28] X. K. Chen, J. C. Irwin, and J. P. Franck, Phys. Rev. B **52**, R13130 (1995).
[29] C. C. Homes, M. Ziaei, B. P. Clayman, J. C. Irwin, and J. P. Franck, Phys. Rev. B **51**, 3140 (1995).
[30] A. B. Kuz'menko, D van der Marel, P. J. M. van Bentum, E. A. Tishchenko, C. Presura, and A. A. Bush, Phys. Rev. B **63**, 094303 (2001).
[31] U. Kuhlmann, C. Thomsen, A. V. Prokofiev, F. Büllesfeld, E. Uhrig, M. Anton, C. Gross, and W. Assmus, Phys. Status Solidi A **196**, 185 (2003).
[32] A. B. Sushkov, O. Tchernyshyov, W. Ratcliff, S. W. Cheong, and H. D. Drew, Phys. Rev. Lett. **94**, 137202 (2005).
[33] G. Caimi, L. Degiorgi, H. Berger, and L. Forró, Europhys. Lett. **75**, 496 (2006).
[34] J. Kim, S. Jung, M. S. Park, S. I. Lee, H. D. Drew, H. Cheong, K. H. Kim, and E. J. Choi, Phys. Rev. B **74**, 052406 (2006).
[35] J. Vermette, S. Jandl, and M. M. Gospodinov, J. Phys.: Condens. Matter **20**, 425219 (2008).
[36] K. Sparta *et al.*, Eur. Phys. J. B **19**, 507 (2001).
[37] H. Kageyama, K. Onizuka, T. Yamauchi, and Y. Ueda, J. Cryst. Growth **206**, 65 (1999).
[38] C. C. Homes, M. Reedyk, D. Crandles, and T. Timusk, Appl. Opt. **32**, 2972 (1993).
[39] C. C. Homes, J. M. Tranquada, and D. J. Buttrey, Phys. Rev. B **75**, 045128 (2007).
[40] M. Dressel and G. Grüner, *Electrodynamics of Solids* (Cambridge University Press, Cambridge, 2001).
[41] K. Parlinski, Z-. Q. Li, and Y. Kawazoe, Phys. Rev. Lett. **78**, 4063 (1997).
[42] D. J. Singh, *Planewaves, Pseudopotentials and the LAPW Method* (Kluwer Academic, Boston, 1994).
[43] D. J. Singh, Phys. Rev. B **43**, 6388 (1991).
[44] P. Blaha, K. Schwarz, G. K. H. Madsen, D. Kvasnicka, and J. Luitz, WIEN2K, an augmented plane wave plus local orbitals program for calculating crystal properties, Techn. Universität Wien, Austria, 2001.
[45] W. Baltensperger, J. Appl. Phys. **41**, 1052 (1970).
[46] C. J. Fennie and K. M. Rabe, Phys. Rev. Lett. **96**, 205505 (2006).
[47] F. D. Murnaghan, Proc. Natl. Acad. Sci. U.S.A. **30**, 244 (1944).
[48] S. V. Dordevic (private communication).
[49] K. Parlinksi, software PHONON, 2003.
[50] J. F. Scott, Phys. Rev. B **4**, 1360 (1971).
[51] B. D. Gaulin (private communication).
[52] A. Gozar (private communication).